JOURNAL OF
# Applied Polymer
SCIENCE

## Special Issue: Polymers for Microelectronics

**Guest Editors:** Dr Brian Knapp (Promerus LLC) and
Prof. Paul A. Kohl (Georgia Institute of Technology)

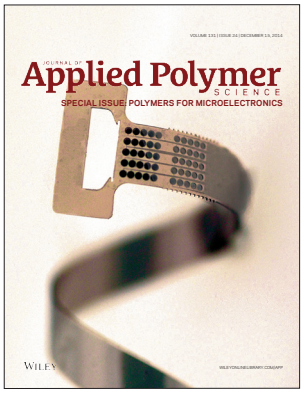


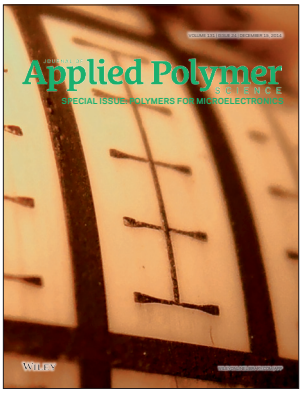


### EDITORIAL

**Polymers for Microelectronics**
B. Knapp and P. A. Kohl, *J. Appl. Polym. Sci.* 2014, **DOI: 10.1002/app.41233**

### REVIEW

**Negative differential conductance materials for flexible electronics**
A. Nogaret, *J. Appl. Polym. Sci.* 2014, **DOI: 10.1002/app.40169**

### RESEARCH ARTICLES

**Generic roll-to-roll compatible method for insolubilizing and stabilizing conjugated active layers based on low energy electron irradiation**
M. Helgesen, J. E. Carlé, J. Helt-Hansen, A. Miller, and F. C. Krebs, *J. Appl. Polym. Sci.* 2014, **DOI: 10.1002/app.40795**

**Selective etching of polylactic acid in poly(styrene)-block-poly(D,L)lactide diblock copolymer for nanoscale patterning**
C. Cummins, P. Mokarian-Tabari, J. D. Holmes, and M. A. Morris, *J. Appl. Polym. Sci.* 2014, **DOI: 10.1002/app.40798**

**Preparation and dielectric behavior of polyvinylidene fluoride composite filled with modified graphite nanoplatelet**
P. Xie, Y. Li, and J. Qiu, *J. Appl. Polym. Sci.* 2014, **DOI: 10.1002/app.40229**

**Design of a nanostructured electromagnetic polyaniline–Keggin iron–clay composite modified electrochemical sensor for the nanomolar detection of ascorbic acid**
R. V. Lilly, S. J. Devaki, R. K. Narayanan, and N. K. Sadanandhan, *J. Appl. Polym. Sci.* 2014, **DOI: 10.1002/app.40936**

**Synthesis and characterization of novel phosphorous-silicone-nitrogen flame retardant and evaluation of its flame retardancy for epoxy thermosets**
Z.-S. Li, J.-G. Liu, T. Song, D.-X. Shen, and S.-Y. Yang, *J. Appl. Polym. Sci.* 2014, **DOI: 10.1002/app.40412**

**Electrical percolation behavior and electromagnetic shielding effectiveness of polyimide nanocomposites filled with carbon nanofibers**
L. Nayak, T. K. Chaki, and D. Khastgir, *J. Appl. Polym. Sci.* 2014, **DOI: 10.1002/app.40914**

**Morphological influence of carbon modifiers on the electromagnetic shielding of their linear low density polyethylene composites**
B. S. Villacorta and A. A. Ogale, *J. Appl. Polym. Sci.* 2014, **DOI: 10.1002/app.41055**

**Electrical and EMI shielding characterization of multiwalled carbon nanotube/polystyrene composites**
V. K. Sachdev, S. Bhattacharya, K. Patel, S. K. Sharma, N. C. Mehra, and R. P. Tandon, *J. Appl. Polym. Sci.* 2014, **DOI: 10.1002/app.40201**

**Anomalous water absorption by microelectronic encapsulants due to hygrothermal-induced degradation**
M. van Soestbergen and A. Mavinkurve, *J. Appl. Polym. Sci.* 2014, **DOI: 10.1002/app.41192**

**Design of cyanate ester/azomethine/$ZrO_2$ nanocomposites high-k dielectric materials by single step sol-gel approach**
M. Ariraman, R. Sasi Kumar and M. Alagar, *J. Appl. Polym. Sci.* 2014, **DOI: 10.1002/app.41097**

**Furan/imide Diels–Alder polymers as dielectric materials**
R. G. Lorenzini and G. A. Sotzing, *J. Appl. Polym. Sci.* 2014, **DOI: 10.1002/app.40179**

**High dielectric constant polyimide derived from 5,5'-bis[(4-amino) phenoxy]-2,2'-bipyrimidine**
X. Peng, Q. Wu, S. Jiang, M. Hanif, S. Chen, and H. Hou, *J. Appl. Polym. Sci.* 2014, **DOI: 10.1002/app.40828**

**The influence of rigid and flexible monomers on the physical-chemical properties of polyimides**
T. F. da Conceição and M. I. Felisberti, *J. Appl. Polym. Sci.* 2014, **DOI: 10.1002/app.40351**

JOURNAL OF
Applied Polymer
SCIENCE

# Special Issue: Polymers for Microelectronics

**Guest Editors:** Dr Brian Knapp (Promerus LLC) and
Prof. Paul A. Kohl (Georgia Institute of Technology)

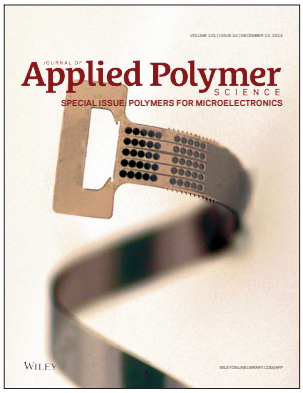


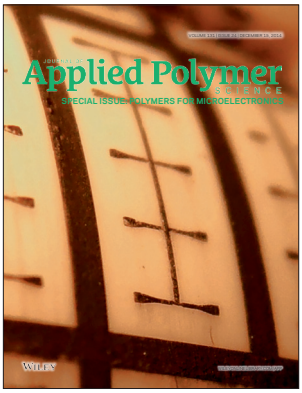


**Development of polynorbornene as a structural material for microfluidics and flexible BioMEMS**
A. E. Hess-Dunning, R. L. Smith, and C. A. Zorman, *J. Appl. Polym. Sci.* 2014, **DOI:** 10.1002/app.40969

**A thin film encapsulation layer fabricated via initiated chemical vapor deposition and atomic layer deposition**
B. J. Kim, D. H. Kim, S. Y. Kang, S. D. Ahn, and S. G. Im, *J. Appl. Polym. Sci.* 2014, **DOI:** 10.1002/app.40974

**Surface relief gratings induced by pulsed laser irradiation in low glass-transition temperature azopolysiloxanes**
V. Damian, E. Resmerita, I. Stoica, C. Ibanescu, L. Sacarescu, L. Rocha, and N. Hurduc, *J. Appl. Polym. Sci.* 2014, **DOI:** 10.1002/app.41015

**Polymer-based route to ferroelectric lead strontium titanate thin films**
M. Benkler, J. Hobmaier, U. Gleißner, A. Medesi, D. Hertkorn, and T. Hanemann, *J. Appl. Polym. Sci.* 2014, **DOI:** 10.1002/app.40901

**The influence of dispersants that contain polyethylene oxide groups on the electrical resistivity of silver paste**
T. H. Chiang, Y.-F. Chen, Y. C. Lin, and E. Y. Chen, *J. Appl. Polym. Sci.* 2014, **DOI:** 10.1002/app.41183

**Quantitative investigation of the adhesion strength between an SU-8 photoresist and a metal substrate by scratch tests**
X. Zhang, L. Du, and M. Zhao, *J. Appl. Polym. Sci.* 2014, **DOI:** 10.1002/app.41108

**Thermodynamic and kinetic aspects of defectivity in directed self-assembly of cylinder-forming diblock copolymers in laterally confining thin channels**
B. Kim, N. Laachi, K. T. Delaney, M. Carilli, E. J. Kramer, and G. H. Fredrickson, *J. Appl. Polym. Sci.* 2014, **DOI:** 10.1002/app.40790

Journal of Applied Polymer Science

# Quantitative Investigation of the Adhesion Strength Between an SU-8 Photoresist and a Metal Substrate by Scratch Tests

**Xiaolei Zhang,[1] Liqun Du,[1,2] Ming Zhao[1]**

[1]Key Laboratory for Precision & Non-Traditional Machining Technology of Ministry of Education, Dalian University of Technology, Dalian 116024, China

[2]Key Laboratory for Micro/Nano Technology and System of Liaoning Province, Dalian University of Technology, Dalian 116024, China

Correspondence to: L. Du (E-mail: duliqun@dlut.edu.cn)

**ABSTRACT:** During the manufacturing process of metal microstructures and microdevices by SU-8 ultraviolet-lithographie, galanoformung and abformung (UV–LIGA) technology, interfacial delamination and bond failure are common because of the poor adhesion strength between the SU-8 photoresist and the metal substrate. In this study, a scratch method was used to measure the adhesion strength between the SU-8 and the metal substrate. A simulation of a scratch test process was accomplished on the basis of the finite element method, and a modified empirical formula that accounted for local horizontal stress was deduced by a dimensional analysis method. The good agreement among the calculated formula, corresponding simulant, and experimental results showed the validity of the modified empirical formula. Interfacial adhesion work was also obtained to characterize the interfacial adhesion properties. This study provided a theoretical basis for quantitatively estimating the interfacial adhesion strength and a theoretical foundation for improving the interfacial adhesion properties. © 2014 Wiley Periodicals, Inc. J. Appl. Polym. Sci. **2014**, *131*, 41108.

**KEYWORDS:** films; surfaces and interfaces; theory and modeling

Received 19 February 2014; accepted 16 June 2014

**DOI: 10.1002/app.41108**

## INTRODUCTION

The SU-8 photoresist is a negative, epoxy-type, near-UV photoresist first developed by IBM, and it is commonly used for the fabrication of high-aspect-ratio microstructures and microdevices.[1] With the increasing requirements for metal microstructures and microdevices, the metal is directly applied as a substrate because of its advantages of lower processing, short electroforming time, and indestructibility.[2,3] However, the poor adhesion strength between the SU-8 photoresist and the metal substrate seriously affects the product yield and stability of microstructures and microdevices.[4] Therefore, it is worth investigating the adhesion strength between the SU-8 photoresist and the metal substrates.

The investigation of the adhesion properties is based on an appropriate measurement method. Some methods are used to assess the film adhesion, such as the pull-off method,[4] peel method,[5] interfacial indentation test,[6] indentation test,[7] and scratch test.[8–12]

During the scratch test, a diamond indenter is drawn across the film surface under an increasing load until film detachment occurs, where a critical load is used to assess the interfacial adhesion strength.[8] However, critical loads are strongly affected by various parameters, including the film thickness ($t$) and scratch speed,[13] and these fail to accurately characterize the interfacial adhesion strength. Therefore, other parameters need to be considered to characterize the interfacial adhesion strength, such as the shear stress at the critical load[14–16] and the practical interfacial adhesion work ($W$).[8]

Over the past few decades, the adhesion strengths of various film–substrate interfaces have been investigated by scratch testing, and corresponding analytical models have been built.

Benjamin and Weaver[14] first established scratch test models, including a tangential force model and a normal force model. The tangential force model was applied to calculate the interfacial adhesion strength between a thin film (e.g., Ag, Au, Pt, Sn) and a transparent substrate (e.g., glass, Perspex, polystyrene, NaCl). However, this model ignores the elastic deformation of the film and is only suitable for the case in which the film is penetrated through completely. The normal force model was used to calculate the interfacial adhesion strength between the metal film and the glass substrate. In this model, the thickness of the film was ignored. It was considered that the thin and ductile film was deformed to contour the shape of the indenter,

© 2014 Wiley Periodicals, Inc.

and the substrate surface was plastically deformed during the loading. However, this full plastic method has some limitations.

Laugier[16] used shear stress to characterize the interfacial adhesion strength as well. However, Laugier's model only considers the elastic deformation and is suitable for the film (e.g., brittle film), where only elastic deformation occurs when the interface is separated. For the ductile film, elastic and plastic deformations both occur in the film, and the model is not applicable in this case.

Then, Laugier[8,17] described the removal process of the film by the indenter from the point of view of energy. *W* was adopted to characterize the interfacial adhesion strength. Laugier made some analyses and calculations. However, because the plastic deformation was neglected, the deduced model also could not properly describe the stress in the film.

The differences in the scratch features at the film–substrate interface resulted in various scratch models. Some researchers have improved the aforementioned models to make them adaptable to specific interfaces.

On the basis of the normal force model of Benjamin and Weaver,[14] Ollivier and Matthews[15] established the model used in the scratch test of the interface of the hard film–soft substrate (e.g., diamond-like carbon film and polymer substrate). However, because of the effect of substrate deformation, this model cannot give an absolute value of the interfacial shear strength and can only be a semiquantities model.

Burnett and Rickerby[18,19] considered the elastic and plastic deformations around the indenter. On the basis of their investigation, Attar and Johannesson[20] and Staia et al.[21] established the relationship between the critical load and *W*. However, their model only adapts to the case of small coefficient of friction.

On the basis of the investigation of Burnett and Rickerby,[18,19] Bull et al.[22] established the relationship between the critical load and *W* by considering the effect of the friction coefficient. However, this model only adapts to test the interfacial adhesion strength of the hard film–soft substrate. In addition, Bull thought that, in this model, the indentation depth ($h$) should be two times more than $t$.

In the model establishment process, the toughness or brittleness of the film, the elastic and plastic deformations of the film, the hardness of the substrate, and $h$ (e.g., whether the film is penetrated through) should be taken into account. For the interface of the SU-8 photoresist and the metal substrate, the film is an elastic–perfectly plastic material film, and the substrate is hard compared with the film. During the practical scratch test, elastic and plastic deformations occurred in the SU-8 photoresist film. In addition, experimental observation showed that the film was not penetrated through completely at the critical load. Until now, there has been no model to compatibly describe the interfacial adhesion strength between the SU-8 photoresist and the metal substrate. Therefore, it is necessary to establish a corresponding theoretical model for quantitatively estimating the interfacial adhesion strength and to provide a theoretical foundation for improving the interfacial adhesion properties.

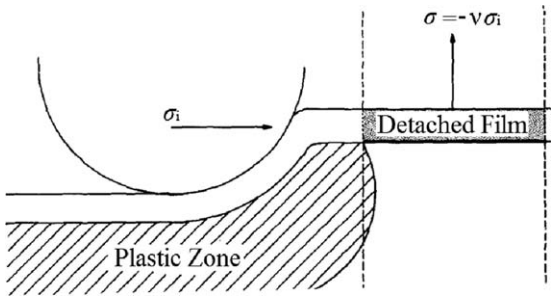


**Figure 1.** Schematic diagram of the stress distribution ahead of the indenter responsible for the film.

In this study, a scratch test was adopted to measure the interfacial adhesion strength between the SU-8 photoresist and the metal substrate. On the basis of the hypothesis that the stress field at the head of indenter was composed of a Boussinesq field, a Blister field, and a friction field, the scratch test model was established by finite element simulation and a dimensional analysis method. *W* was adopted to characterize the adhesion strength between the SU-8 photoresist and the metal substrate.

## INTERFACIAL ADHESION STRENGTH

As Laugier[8,17] proposed, the adhesion behavior can be modeled in terms of the strain energy released during the removal of a film. At the critical load, the interfacial failure predominantly occurs ahead of the moving indenter, where the compressive stresses are at a maximum. The film ahead of the indenter can thus reduce the elastic energy stored in it by buckling or spalling from the substrate at the critical load. The magnitude of the stresses responsible for the film removal can be determined by the Griffith energy balance approach. Figure 1 shows the stress distribution ahead of the indenter responsible for film detachment. Under uniaxial tension, the elastic strain energy per unit volume ($U_e$) is given by

$$U_e = \frac{\sigma^2}{2E} \tag{1}$$

where $\sigma$ is the stress perpendicular to the interface in the elastic field and $E$ is the Young's modulus of the film. It is considered that at the critical load, a semicircular film with radius $b$ detaches from the substrate. With the elastic effects of the substrate ignored, the elastic strain energy released from the semicircular film is given by

$$U_r = \frac{\pi b^2 t}{2} \times \frac{1}{2} \times \frac{\sigma^2}{E} \tag{2}$$

The elastic strain energy released from the semicircular film provides the surface energy for the interfacial crack and can be characterized by *W*:

$$W = \gamma_s + \gamma_f - \gamma_{sf} \tag{3}$$

where $\gamma_s$ and $\gamma_f$ are the surface energies of the substrate and film, respectively, and $\gamma_{sf}$ is the interfacial energy. Balancing the released elastic energy to the surface energy of the crack

$$\frac{\pi b^2 t}{2} \times \frac{1}{2} \times \frac{\sigma^2}{E} = \frac{\pi b^2}{2} \times W \tag{4}$$

Equation (4) can be simplified to

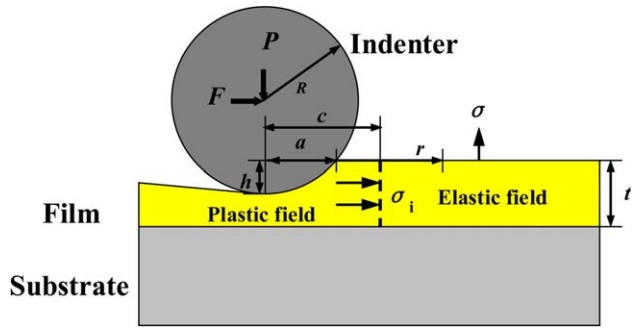


**Figure 2.** Schematic of the thick film–hard substrate system scratch test. [Color figure can be viewed in the online issue, which is available at wileyonlinelibrary.com.]

$$W=\frac{1}{2}\times\frac{\sigma^2 t}{E} \tag{5}$$

According to the Poisson effect, eq. (5) is given by

$$W=\frac{1}{2}\times\frac{\sigma^2 t}{E}=\frac{v^2\sigma_i^2 t}{2E} \tag{6}$$

where $\sigma_i$ is the compressive horizontal stress parallel to the interface in the film–substrate system, $v$ is the Poisson ratio of the film material, and $\sigma = v\sigma_i$.

This model is usually used in the situation where the thickness of the film is smaller than the indenter size. However, for a thick film, the indenter fails to penetrate through the film. During the loading of the indenter, elastic and plastic deformations of the film occur without debonding until a critical vertical load of the film–substrate system ($P$) is reached. Then, the interfacial fracture initiates from the elastic–plastic interfacial position ($c$).[23] Additionally, our following simulation results show that $\sigma_i$ approximately parallels with the film–substrate interface and is perpendicular to the elastic–plastic interface. Therefore, eq. (6) is still applicable for the calculation of $W$. Figure 2 is the schematic of a thick film–hard substrate system scratch test.

$\sigma_i$ is significant for the calculation of $W$. For the block material, the stress distribution field ahead of the indenter consisted of a Boussinesq field, a Blister field, and a friction traction field in the scratch test.[24] Corresponding stresses included the elastic indentation stress, or Boussinesq stress, of the block material ($\sigma_{B,o}$); the stress after plastic deformation, or Blister stress, of the block material ($\sigma_{Bl,o}$); and the tangential frictional stress of the block material ($\sigma_{f,o}$). According to the Boussinesq solution for a point load on the flat surface of a semi-infinite half-space, $\sigma_{B,o}$ is given by[25]

$$\sigma_{B,o}=\frac{P_o}{2\pi r^2}(1-2v) \tag{7}$$

where $P_o$ is the critical vertical load of the block material, and $r$ is the distance between the point ahead of the indenter and the central axle of indenter, as shown in Figure 2. $\sigma_{Bl,o}$ is given by[25]

$$\sigma_{Bl,o}=\frac{4B_o(2-v)}{r^3} \tag{8}$$

where $B_o$ is a constant, a measure of the field strength. It is obtained by the stress continuity method:[26]

$$B_o=\frac{P_o r(2v^2-v+1)}{8\pi(v-1)(v-2)} \tag{9}$$

$\sigma_{Bl,o}$ is obtained by substituting eq. (9) into eq. (8):

$$\sigma_{Bl,o}=\frac{P_o}{2\pi r^2}\times\frac{(2v^2-v+1)}{(v-1)} \tag{10}$$

Friction stress[27] is given by

$$\sigma_{f,o}=\frac{3F_o}{2\pi a^3 r^3}\left(2r^2G_o-vM_o\right) \tag{11}$$

where

$$G_o=\frac{1}{2}a\left(r^2-a^2\right)^{1/2}+\frac{1}{2}r^2\ \arctan\left[a\left(r^2-a^2\right)^{-1/2}\right] \tag{12}$$

$$M_o=\frac{1}{2}a\left(r^2-a^2\right)^{3/2}-\frac{1}{4}r^4\ \arctan\left[a\left(r^2-a^2\right)^{-\frac{1}{2}}\right]-\frac{1}{4}ar^2\left(r^2-a^2\right)^{\frac{1}{2}} \tag{13}$$

where $G_o$ and $M_o$ are constants. The compressive horizontal stress in the local block material ($\sigma_{i,o}$) is obtained by the superimposition of these three types of stress, which is written as follows:

$$\sigma_{i,o}=\sigma_{B,o}+\sigma_{Bl,o}+\sigma_{f,o} \tag{14}$$

For a film–substrate system, because of the constraints of the substrate, $\sigma_i$ is related to the ratio of $h$ to $t$. In consideration of another relative parameter, the indenter radius ($R$), $\sigma_i$ can be written as a function of the dimensionless $h/t$ and $R/t$:

$$\sigma_i=g\left(\frac{h}{t}\right)\times f\left(\frac{R}{t}\right)\left(\sigma_{B,o}+\sigma_{Bl,o}+\sigma_{f,o}\right) \tag{15}$$

where $g$ and $f$ are the functions of $h/t$ and $R/t$, respectively. For convenience, $P_o$ and the horizontal load of the block film material ($F_o$) are substituted by $P$ and the horizontal load in the film–substrate system ($F$), respectively.

During sphere indenter loading, $P$ and $P_o$ are given by[28]

$$P=\frac{4a^2}{k}H \tag{16}$$

$$P_o=\frac{4a^2}{k_o}H_o \tag{17}$$

where $H$ is the hardness of the film affected by the substrate and $H_o$ is the hardness of the block film material obtained by scratch test. $4a^2/k$ and $4a^2/k_o$ (where $k$ and $k_o$ are parameters that refer to the indentation area) are the contact areas between the indenter and the film for the film–substrate system and the block film material, respectively. Obviously, $k$ is relative to the indentation radius ($a$), $R$, $h$, and $t$, whereas $k_o$ is relative to $a$ and $R$. Therefore, $k$ is a function ($T$) of $a$, $R$, $h$, and $t$ and $k_o$ is a function ($Q$) of $a$ and $R$:

$$k=\frac{4a^2H}{P}=T\left(\frac{h}{t},\frac{a}{R}\right) \tag{18}$$

$$k_o=\frac{4a^2H_o}{P_o}=Q\left(\frac{a}{R}\right) \tag{19}$$

$k$ and $k_o$ can be obtained by the calculation of the contact areas in the simulation. When $a$, $R$, and $H$ and $a$, $R$, $P_o$, and $H_o$ are inserted into eqs. (18) and (19), respectively, $T$ and $Q$ can be obtained by a dimensional analysis method, and then $k$ and $k_o$ can be obtained.

Bhattacharya and Nix[29] investigated the effect of the substrate on the measurement of the film hardness in a soft film–hard substrate system and performed a finite element simulation of indentation process with a pyramid-shaped indenter. Bhattacharya and Nix obtained the film hardness by fitting the simulation results. The results show that the film hardness was relative to the ratio of $h$ to $t$. However, for the sphere indenter, the ratio of $a$ to $h$ during loading changed rather than remaining constant for the pyramid indenter. That means the film hardness was also relative to the indenter size for the sphere indenter. Therefore, the relationship between $H$ and $H_o$ is given by

$$\frac{H}{H_o}=U\left(\frac{h}{t}\right)\times V\left(\frac{a}{R}\right) \tag{20}$$

The functions $U$ and $V$ are obtained by the dimensional analysis method, and then, eq. (21) is given on the basis of eqs. (16) and (17):

$$P_o=\frac{kH_o}{k_oH}P \tag{21}$$

When $h$ is not too deep, $F$ approximates $F_o$ for the same $h$, that is, $F \approx F_o$. When $P_o$ and $F_o$ are substituted in eq. (7), eqs. (10) and (11) for $P$ and $F$, with $c$ for $r$ substituted, $\sigma_i$ is given by

$$\begin{cases} \sigma_i=g\left(\frac{h}{t}\right)\times f\left(\frac{R}{t}\right)\left(\sigma_{B,o}+\sigma_{Bl,o}+\sigma_{f,o}\right) \\ \sigma_B=\frac{kH_oP}{2\pi c^2k_oH}(1-2v) \\ \sigma_{Bl}=\frac{kH_oP}{2\pi c^2k_oH}\times\frac{(2v^2-v+1)}{(v-1)} \\ \sigma_f=\frac{3F}{2\pi a^3c^3}\left(2c^2G_o-vM_o\right) \end{cases} \tag{22}$$

where $\sigma_B$, $\sigma_{Bl}$, and $\sigma_f$ are the Boussinesq stress, Blister stress, and tangential frictional stress in the film–substrate system, respectively. With insertion of $t$, $h$, $R$, $P$, and $F$ and other material parameters into eq. (22), $\sigma_i$ is obtained by the dimensional analysis method, and then, $W$ is obtained.

## SIMULATION INVESTIGATION

Because it is difficult to measure the stress distribution of the film directly by experiments in the scratch test, the stress distributions of the film–substrate system and the block material were simulated by the finite element package ANSYS in this study.

First, the scratch system was simplified. Because the SU-8 photoresist is softer compared to most metals, the metal substrate was assumed to be rigid, and the system was a soft film–hard substrate system. After the postbake cooling process, the cross-linked SU-8 photoresist was in the glass state and could be assumed to be an elastic material.[30] Therefore, in this study, the viscoelasticity of the SU-8 photoresist film was ignored. The film was assumed to be an elastic–perfectly plastic material with the stress–strain relationship. In the simulation, the film was supported by the constraint of the lower surface nodes. Figure 3(a) shows a three-dimensional finite element analysis model of the scratch test, in which a rigid sphere indenter with a radius of 200 $\mu$m was loaded onto the SU-8 photoresist film. Symmetrical conditions were applied to the model below the indenter.

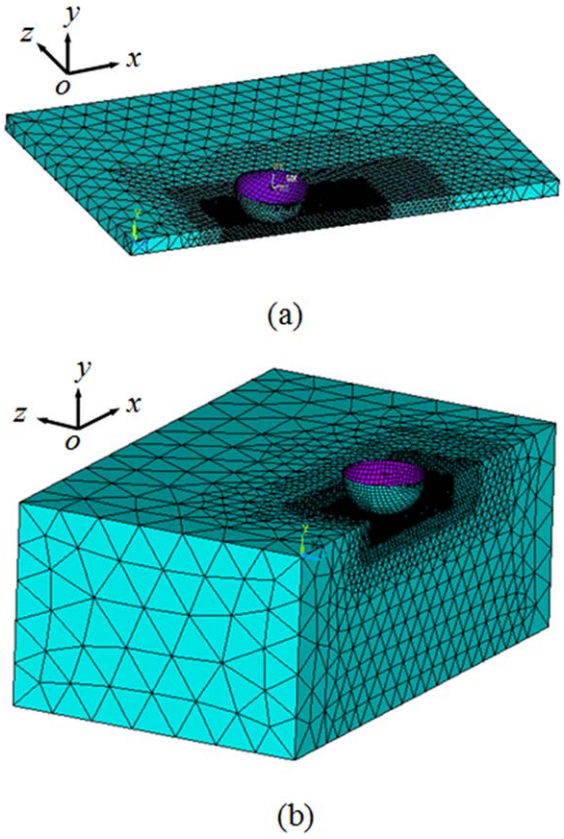


**Figure 3.** Simulant model of the scratch test on the (a) film–substrate system and (b) block material. [Color figure can be viewed in the online issue, which is available at wileyonlinelibrary.com.]

The film was meshed by VISCO107 elements with a free meshing method. Local mesh refinement around the scratch was performed by three successive steps so that the grid was dense under the indenter and sparse apart from the indenter. The contact pairs were meshed by TARGEL170 and CONTAL175 elements. A model with a length of 2500 $\mu$m ($x$ direction, or scratch direction) and a width of 2000 $\mu$m ($z$ direction, or perpendicular to the scratch direction and parallel to the film–substrate interface) was established, and the thickness was in the $y$ direction (or the $t$ direction). The material parameters were as follows: Young's modulus of the SU-8 photoresist was 3.09 GPa, $v$ was 0.22, and the stress–strain curve was assured, as indicated in ref. 31. The experimental scratch distance was more than 1500 μm and could not be fully calculated because it would require a model size that was too large and a very long computation time. The calculation was performed by two steps: first, a vertical displacement to the indenter was imposed until an $h$ ranging from 9 to 45 $\mu$m was obtained (the indentation step). Second, a horizontal translation at a constant depth was imposed to the indenter until the desired scratch distance was obtained (the scratch step). Some preliminary computations with the highest penetration depth (45 $\mu$m) showed that the calculation required a minimum scratch distance of 300 μm to reach a stationary state. The scratch distance was then chosen as 400 $\mu$m. The global dimensions of the model were carefully

**Table I.** Results of Simulation

| $t$ ($\mu$m) | $h$ ($\mu$m) | $P$ (N) | $F$ (N) | $c$ ($\mu$m) | $a$ ($\mu$m) | $H$ (MPa) | $P_o$ (N) | $k$ | $k_o$ | $\sigma_i$ FEM (MPa) | $\sigma_{i,o}$ FEM (MPa) |
|---|---|---|---|---|---|---|---|---|---|---|---|
| 60 | 9.0 | 2.24 | 0.20 | 102.25 | 59.32 | 228.83 | 2.12 | 1.467 | 1.326 | 19.76 | 15.90 |
| | 12.0 | 3.03 | 0.35 | 160.19 | 68.23 | 477.89 | 2.89 | 1.586 | 1.369 | 21.86 | 12.90 |
| | 15.0 | 4.39 | 0.71 | 236.67 | 75.99 | 477.89 | 3.62 | 1.959 | 1.408 | 22.31 | 8.30 |
| | 18.0 | 6.41 | 1.55 | 324.88 | 82.92 | 477.89 | 3.91 | 2.067 | 1.486 | 23.74 | 7.40 |
| 90 | 13.5 | 3.46 | 0.58 | 142.29 | 72.23 | 243.99 | 3.32 | 1.423 | 1.398 | 21.47 | 21.30 |
| | 18.0 | 4.92 | 1.32 | 211.12 | 82.92 | 305.45 | 3.91 | 1.647 | 1.486 | 23.42 | 17.10 |
| | 22.5 | 7.96 | 2.59 | 305.12 | 92.16 | 448.00 | 4.58 | 1.903 | 1.518 | 26.28 | 13.30 |
| | 27.0 | 10.42 | 4.19 | 406.18 | 100.35 | 543.02 | 5.17 | 2.080 | 1.742 | 28.01 | 14.70 |
| 120 | 18.0 | 5.11 | 1.50 | 204.66 | 82.92 | 278.31 | 3.91 | 1.555 | 1.486 | 22.73 | 22.50 |
| | 24.0 | 7.32 | 2.50 | 266.92 | 94.99 | 351.78 | 4.82 | 1.732 | 1.594 | 24.68 | 21.60 |
| | 30.0 | 9.35 | 3.92 | 371.11 | 105.36 | 408.99 | 5.39 | 2.021 | 1.870 | 27.61 | 17.30 |
| | 36.0 | 12.56 | 5.89 | 459.62 | 114.47 | 510.59 | 5.78 | 2.087 | 1.903 | 29.64 | 13.76 |
| 150 | 22.5 | 6.69 | 2.67 | 252.80 | 92.16 | 298.43 | 4.58 | 1.557 | 1.518 | 26.07 | 25.20 |
| | 30.0 | 9.43 | 3.77 | 318.06 | 105.36 | 372.83 | 5.39 | 1.649 | 1.870 | 27.17 | 22.70 |
| | 37.5 | 12.49 | 6.38 | 417.06 | 116.59 | 451.58 | 6.12 | 2.080 | 1.953 | 29.67 | 17.60 |
| | 45.0 | 16.34 | 6.74 | 513.11 | 126.39 | 551.36 | 6.90 | 2.108 | 2.044 | 31.97 | 16.59 |

chosen to prevent edge effects that might have perturbed the calculation.[32] The indentation stress ahead of the indenter and the reaction forces were detected by a postprocessor. To acquire $\sigma_i$, all nodes on the symmetric plane of the model, on which the von Mises stress was equal to the material uniaxial yield stress, were picked. The principle stress of these nodes along the scratch direction was $\sigma_i$. The distance between these nodes and the central axis was approximately $c$.

Second, the scratch process on the block material, that is, the nonsubstrate condition, was simulated. To construct a semi-infinite half-space, the thickness of the model in the $y$ direction was set as 2000 $\mu$m, as shown in Figure 3(b). The model was supported by the constraint of the lower surface nodes. The settings of the other parameters were similar to those in the film–substrate system. After loading and solution, $\sigma_i$ in the elastic–plastic interface corresponding to the same depth in the film–substrate system was obtained.

The $t$ values were set as 60, 90, 120, and 150 $\mu$m. The ratios of $h$ to $t$ were set as 15, 20, 25, and 30%, and the corresponding $h$ is shown in Table I. The scratch processes in the film–substrate system and the block material in the same $h$ were simulated. The $P$, $F$, and the stress distribution ahead of the indenter were obtained. Figure 4 shows the contour of the principle stress along the $x$ direction. As shown in Figure 4, the elastic–plastic interface (dashed line) was approximately perpendicular to the film–substrate interface.

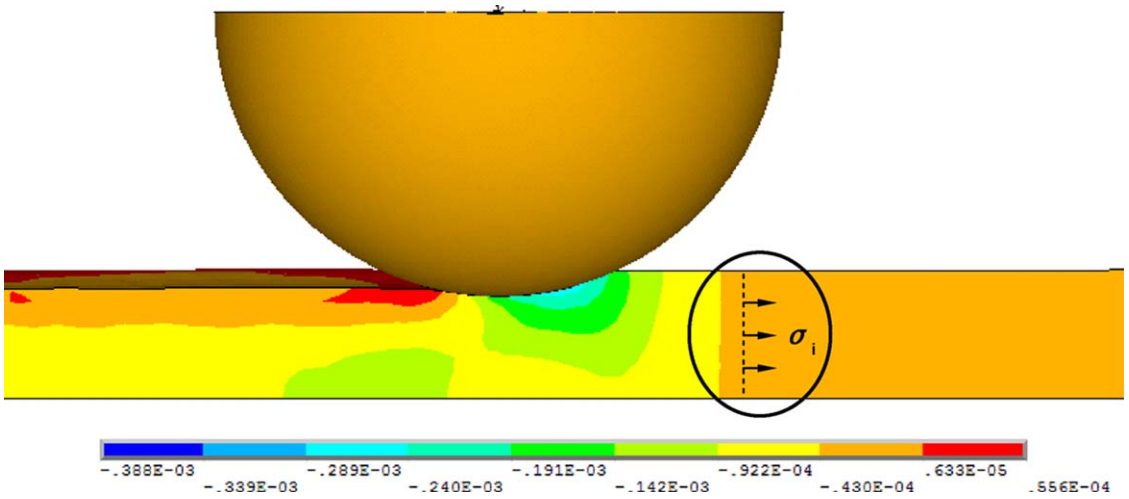


**Figure 4.** Contour of the simulant principle stress in the $x$ direction. [Color figure can be viewed in the online issue, which is available at wileyonlinelibrary.com.]

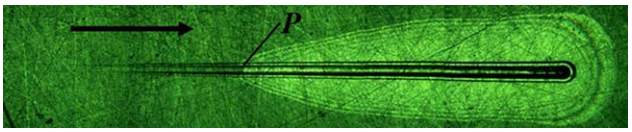


**Figure 5.** View of the scratch morphology. [Color figure can be viewed in the online issue, which is available at wileyonlinelibrary.com.]

## EXPERIMENTAL

To verify the accuracy of the simulation results, corresponding scratch tests were performed on the SU-8 photoresist film and metal substrate system.

Because stainless steel is usually applied to the fabrication of microfluidic devices, such as micro heat exchangers, micro power generators, and micro tool electrodes, which work in high-temperature, high-pressure, or strong corrosion circumstances,[33,34] stainless steel was used as a metal substrate material in this study.

The experimental processes were as follows:

1. We washed 316L stainless steel with acetone, ethanol, and deionized water and then dried it.
2. We spun the SU-8 2075 photoresist (MicroChem Corp.), first at an initial speed of 900 rpm for 10 s and then at a maximum speed of 1200 rpm for 30 s. We then placed the sample on a level surface for 20 min.
3. We prebaked the sample for 3 h at 75°C on a level hot plate and then cooled it down to room temperature.
4. We exposed the sample for 8 min with BGJ-3-type lithography exposure. The total dose was 400 mJ/cm$^2$.
5. We postbaked the sample for 4 min at 85°C on a level hot plate and then cooled it down to room temperature.
6. We completed the developing process with developer (MicroChem Corp.) for 10 min.
7. We measured the thickness of the SU-8 film with an electro-inductance micrometer.
8. We performed the scratch test on the samples with a CSR-1 scratch tester (TB-01 CSR-01, Rhesca Co., Ltd. Japan) under a loading rate of 20 N/min and a scratch rate of 10 mm/min. The maximum load was 10 N, and the scratch length was 10 mm. The indenter was a Rockwell diamond cone with an $R$ of 0.2 mm and a cone angle of 120°. A tool microscope (STM6, Olympus) was applied to observe the scratch feature and to measure the critical debonding position, as shown in Figure 5. The critical scratch width ($d = 2a$) was measured. The critical load was calculated on the basis of the critical position, the loading data, and the displacement data. The curve of the horizontal force versus the vertical load was portrayed according to the data recorded by the scratch test equipment.

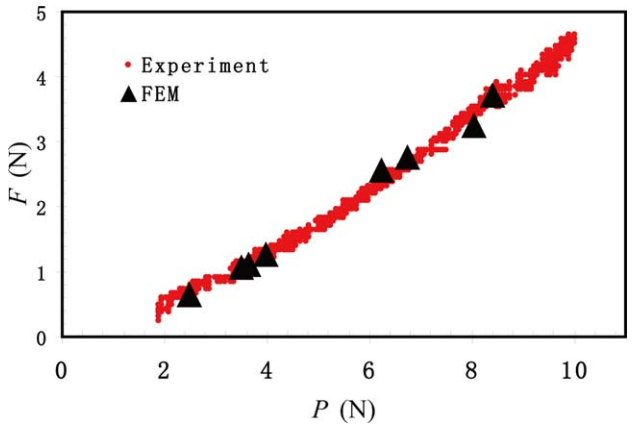


**Figure 6.** Comparison of the horizontal and vertical loads in the simulation within the experiment ($t = 67.4$ $\mu$m). [Color figure can be viewed in the online issue, which is available at wileyonlinelibrary.com.]

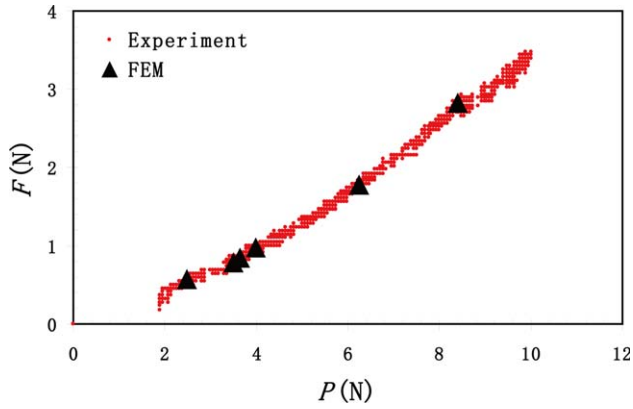


**Figure 7.** Comparison of the horizontal and vertical loads in the simulation within the experiment ($t = 87.8$ $\mu$m). [Color figure can be viewed in the online issue, which is available at wileyonlinelibrary.com.]

## ANALYSIS AND DISCUSSION

The simulation parameters and results, including $t$, $P$, $F$, $h$, $a$, $c$, $\sigma_i$, and $\sigma_{i,o}$, are shown in Table I.

Figures 6 and 7 show the relationship between the horizontal load and vertical load in the experiment and simulation with $t$ values of 67.4 and 87.8 $\mu$m, respectively. The signs • and ▲ represent the experimental and simulation data, respectively. As shown in Figures 6 and 7, the simulation results agreed with the experimental results. This indicated that the simulation model was accurate.

To obtain the relationship between $P$ and $P_o$ in eq. (21), Adobe Photoshop CS (San Jose, CA) image-analysis software was used to evaluate the indentation area through the calculation of image pixels. Then, $k$ and $k_o$ were obtained. Figure 8(a) shows the top view of the scratch indentation. In Figure 8, the round pattern is the indenter, and the pattern inside of the round pattern is the indentation area, only half of which is shown. The indenter symmetry face area was $\pi(200 \times 10^{-6})^2$ $\mu$m$^2$. The pixels of the indentation area and indenter symmetry face area were obtained in the software. According to the following equation, the practical indentation area was obtained:

$$\left(\frac{\text{Indentation area}}{\text{Indenter symmetry face area}}\right)_{\text{Practical}} = \left(\frac{\text{Indentation area}}{\text{Indenter symmetry face area}}\right)_{\text{Pixel}}$$

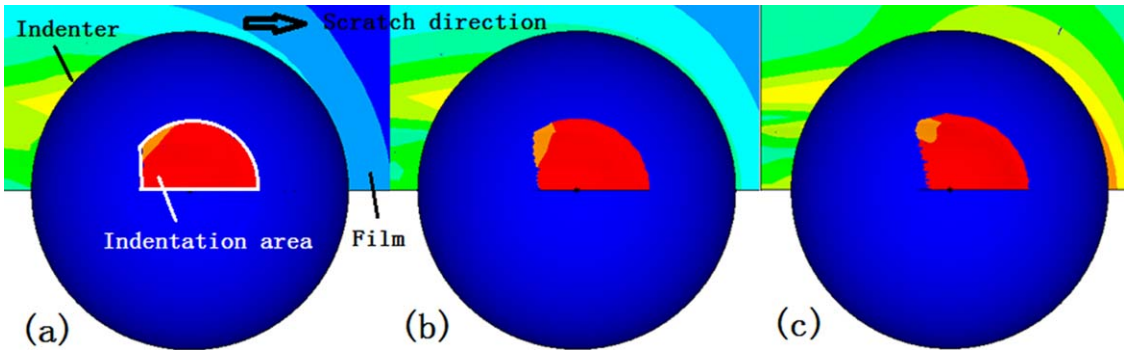


**Figure 8.** Schematic of the indentation area. [Color figure can be viewed in the online issue, which is available at wileyonlinelibrary.com.]

Figure 8(a–c) shows the indentation features of the block material, the film–substrate system with $t$ values of 150 and 90 $\mu$m, respectively. The corresponding indentation areas are listed in Table II. In these three cases, $h$ was 22.5 $\mu$m. As shown in Figure 8 and Table II, because of the effect of the substrate, the indentation areas decreased with $t$ when the other parameters were the same. The results of $k$ are listed in Table I. When $h$, $t$, $R$, and $a$ were inserted into eqs. (18) and (19), the fitting empirical formulas of $k$ and $k_o$ were expressed by

$$k=3.937\left(\frac{h}{t}\right)^{0.455}\left(\frac{a}{R}\right)^{0.118} \tag{23}$$

$$k_o=2.781\left(\frac{a}{R}\right)^{0.688} \tag{24}$$

$H_o$ was measured by the scratch test. The $h$ values were kept less than 10% of $t$ to prevent the effect of the substrate. $H_o$ was obtained from the average of five experimental results. To acquire $H$, according to eq. (20), the data were fitted by the Levenberg–Marquart method, and then, the ratio of $H$ to $H_o$ was obtained:

$$\frac{H}{H_o}=8.422\left(\frac{h}{t}\right)^{0.819}\left(\frac{a}{R}\right)^{0.437} \tag{25}$$

With the substitution of eqs. (23), (24), and (25) into eq. (21), the $P_o$ function represented by $P$ was given as follows:

$$P_o=0.166\left(\frac{h}{t}\right)^{-0.380}\left(\frac{a}{R}\right)^{-0.995}P \tag{26}$$

With the insertion of eq. (26) into eq. (22), $\sigma_i$ was obtained and represented by $P$.

Because it was difficult to determine $c$ directly from the experiment, the relationships among $c$, $a$, $R$, and $t$ were confirmed according to the simulation results. Because $c/a$ could not be less than 1, $c/a$ was fitted and given by

$$\frac{c}{a}=1+8.690\left(\frac{a}{t}\right)^{1.080}\left(\frac{a}{R}\right)^{1.742} \tag{27}$$

With the insertion of eqs. (26) and (27) into eqs. (7–13) and then the insertion of these equations into eq. (14), $\sigma_{i,o}$

**Table II.** Simulation Results of the Indentation Area with Different $t$ Values

| Example | $t$ ($\mu$m) | Indentation area ($\mu$m$^2$) |
|---|---|---|
| In the block material | - | 22,387.8 |
| In the film–substrate system | 150 | 21,822.1 |
| | 90 | 17,851.5 |

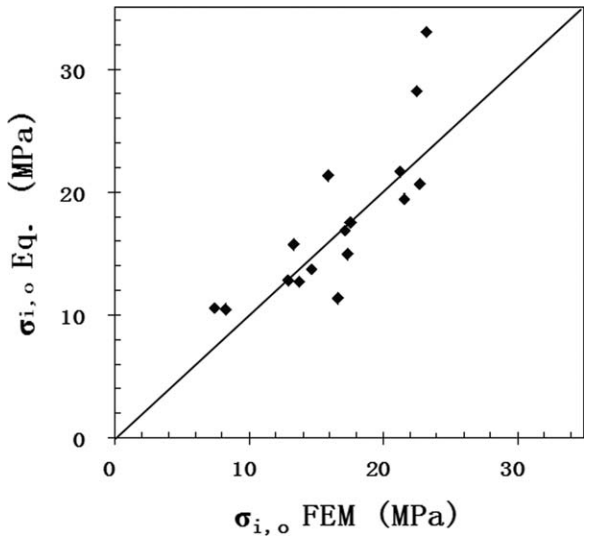


**Figure 9.** Comparison of $\sigma_{i,o}$ from FEM with that from the calculation equation.

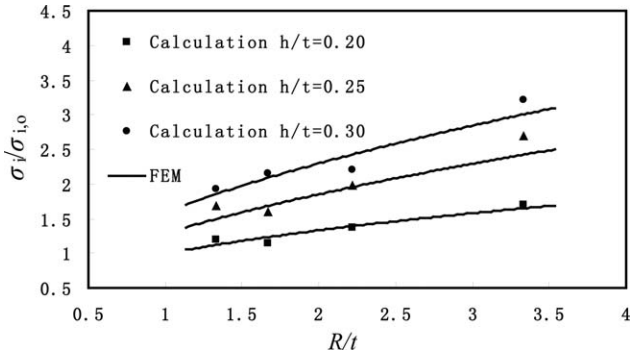


**Figure 10.** Comparison of the FEM results with the calculative results from eq. (29).

**Table III.** Experimental Results of the Scratch Test

| Sample | $P$ (N) | $t$ ($\mu$m) | $F$ (N) | $d$ ($\mu$m) | $h$ ($\mu$m) | $W$ (N/m) | $\bar{W}$ (N/m) |
|---|---|---|---|---|---|---|---|
| 1 | 2.08 | 64.00 | 0.52 | 131.00 | 18.15 | 0.294 | 0.296 |
| | 2.09 | | 0.81 | 140.60 | 17.36 | 0.298 | |
| | 2.08 | | 0.86 | 142.32 | 17.54 | 0.295 | |
| 2 | 4.47 | 90.76 | 1.61 | 166.50 | 22.44 | 0.305 | 0.306 |
| | 4.13 | | 1.48 | 163.00 | 22.62 | 0.308 | |
| | 4.20 | | 1.48 | 163.80 | 25.15 | 0.306 | |
| 3 | 5.16 | 114.00 | 2.55 | 184.10 | 11.03 | 0.291 | 0.292 |
| | 4.96 | | 2.64 | 184.80 | 12.76 | 0.294 | |
| | 5.69 | | 3.18 | 194.20 | 13.09 | 0.290 | |

represented by $P$ and $F$ in the film–substrate system was obtained. With the insertion of $P$, $F$, and other relevant parameters into eq. (14), the $\sigma_{i,o}$ in the block material in the corresponding indentation depths were obtained. The comparison between the simulation results of the film–substrate system and the block material is shown in Figure 9. The abscissa and ordinate represent the simulation result finite element method (FEM) and the theoretical calculation result (eq.), respectively. As shown in Figure 9, most of the data were near the diagonal line, which indicated that the simulation results agreed with the theoretical calculation results. However, a few of data points differed severely at $h/t = 0.15$. This was because when the ratio of $h$ to $t$ was small, the elastic–plastic interface was arc shaped and not vertical to the film–substrate interface. An error occurred in the calculation of the theoretical model.

With the data for $h/t > 0.15$ in Table I inserted into eq. (22) and fitting with the Levenberg–Marquart method, the empirical horizontal stress equation is given by

$$\sigma_c = 6.619\left(\frac{h}{t}\right)^{1.182}\left(\frac{R}{t}\right)^{0.526}\sigma_{i,o} \tag{28}$$

With eq. (26) and eq. (27) inserted into eq. (28)

$$\sigma_c = \frac{1}{2\pi a^3 c^3(v-1)}\left[A\left(2c^2G_o - vM_o\right)F + BvcP\right] \tag{29}$$

where

$$A = 19.857h^{1.182}t^{-1.708}R^{0.506} \tag{30}$$

$$B = -2.198h^{0.802}t^{-1.328}R^{1.518}\left(2Rh-h^2\right)^{1.003} \tag{31}$$

$$c = a + 8.690a^{2.822}t^{-1.080}R^{-1.742} \tag{32}$$

where $A$ and $B$ are the parameters that refer to $\sigma_c$. When we substituted the horizontal stress in the position of the elastic–plastic interface ($\sigma_c$) in eq. (29) for $\sigma_i$ in eq. (6), $W$ was obtained.

Figure 10 shows the relationship between the dimensionless horizontal stress ($\sigma_c/\sigma_{i,o}$) and the ratio of $R$ to $t$. As shown in Figure 10, we observed that the theoretical calculation results agreed with the simulation results; this indicated that eq. (29) was applicable for describing the horizontal stress.

The scratch tests were performed on the film–substrate systems with $t$ values of 64.00, 90.76, and 114.00 $\mu$m. The data of $P$, $t$, $F$, and $d$ were measured in the experiment. $h$ was calculated according to $d$ and $R$. According to eqs. (29) and (6), $W$ between the SU-8 photoresist and the 316L stainless steel substrate and the average interfacial adhesion work ($\bar{W}$) from the average of three experimental results were calculated. The test parameters and the results are listed in Table III.

As shown in Table III, the $W$ values of the three samples were all near 0.3 N/m and were independent of $t$; this indicated that $W$ stably characterized the interfacial adhesion strength between the SU-8 photoresist and the metal substrate.

## CONCLUSIONS

1. On the basis of the assumption of the field ahead of indenter consisting of a Boussinesq field, a Blister field, and a friction traction force field, the scratch test theory model for an elastic–perfectly plastic film–hard substrate system when the film was not penetrated through at the critical load was established. The scratch test was performed to measure the adhesion strength between the SU-8 photoresist and the metal substrate.
2. $W$ was adopted to characterize the adhesion strength between the SU-8 photoresist and the metal substrate. The relationships between $P$ or $F$ and $P_o$ or $F_o$ with the same indentation depths were obtained by a scratch test and finite element simulation. The relationship between $a$ and $c$ was also obtained. Accordingly, the horizontal stress and $W$ were obtained. Moreover, the scratch tests were performed on film–substrate systems with different $t$ values. The results show that the $W$ values were near 0.3 N/m and were independent of $t$. This indicated that $W$ could stably characterize the interfacial adhesion strength between the SU-8 photoresist and the metal substrate.
3. The accuracy of the scratch test theory model was verified by the scratch test. The simulation results agreed with the calculation results of the scratch test theory model. This showed that this scratch test theory model could quantitatively characterize the adhesion strength between the SU-8 photoresist and the metal substrate.

## ACKNOWLEDGMENTS

The authors acknowledge the assistance and encouragement of the National Natural Science Foundation of China (contract grant numbers 51375077, 51075057, and 50675025).

## REFERENCES


1. Hwang, S. F.; Yu, J. H.; Lai, B. J.; Liu, H. K. *Mech. Mater.* **2008**, *40*, 658.
2. Du, L. Q.; Jia, S. F.; Nie, W. R.; Wang, Q. *J. Chin. J. Mech. Eng.* **2011**, *24*, 836.
3. Zhang, X. L.; Du, L. Q.; Xu, Z. *J. Appl. Polym. Sci.* **2012**, *127*, 4456.
4. Dai, W.; Lian, K.; Wang, W. *J. Microsyst. Technol.* **2005**, *11*, 526.
5. Zhang, L.; Wang, J. *Int. J. Adhes. Adhes.* **2009**, *29*, 217.
6. Marot, G.; Démarécaux, P.; Lesage, J.; Hadad, M.; Siegmann, S.; Staia, M. H. *Surf. Coat. Technol.* **2008**, *202*, 4411.
7. Zhang, X. L.; Du, L. Q.; Zhu, Y. L.; Liu, C. *Micro Nano Lett.* **2011**, *6*, 397.
8. Laugier, M. T. *Thin Solid Films* **1984**, *117*, 243.
9. Barnes, D.; Johnson, S.; Snell, R.; Best, S. *J. Mech. Behav. Biomed. Mater.* **2012**, *6*, 128.
10. Covarel, G.; Bensaid, B.; Boddaert, X.; Giljean, S.; Benaben, P.; Louis, P. *Surf. Coat. Technol.* **2012**, *211*, 138.
11. Putkonen, M.; Bosund, M.; Ylivaara, O. M.; Puurunen, R. L.; Kilpi, L.; Ronkainen, H.; Sintonen, S.; Ali, S.; Lipsanen, H.; Liu, X. *Thin Solid Films* **2014**, *558*, 93.
12. Hazra, S.; Bandyopadhyay, P. P. *Mater. Des.* **2014**, *35*, 243.
13. Steinmann, P. A.; Tardy, Y.; Hintermann, H. E. *Thin Solid Films* **1987**, *154*, 333.
14. Benjamin, P.; Weaver, C. In Proceedings of the Royal Society of London Series A. Mathematical and Physical Sciences, Feb **1960**; London: The Royal Society, p 163.
15. Ollivier, B.; Matthews, A. *J. Adhes. Sci. Technol.* **1994**, *8*, 651.
16. Laugier, M. *Thin Solid Films* **1981**, *76*, 289.
17. Laugier, M. T. *J. Mater. Sci.* **1986**, *21*, 2269.
18. Burnett, P. J.; Rickerby, D. S. *Thin Solid Films* **1987**, *154*, 403.
19. Burnett, P. J.; Rickerby, D. S. *Thin Solid Films* **1988**, *157*, 233.
20. Attar, F.; Johannesson, T. *Surf. Coat. Technol.* **1996**, *78*, 87.
21. Staia, M. H.; Puchi, E. S.; Schmutz, C. J. *J. Electron. Mater.* **1997**, *26*, 980.
22. Bull, S. J.; Rickerby, D. S.; Matthews, A.; Leyland, A.; Pace, A. R.; Valli, J. *Surf. Coat. Technol.* **1988**, *36*, 503.
23. Matthewson, M. *J. Appl. Phys. Lett.* **1986**, *49*, 1426.
24. Park, H.; Kwon, D. *Thin Solid Films* **1997**, *307*, 156.
25. Yoffe, E. H. *Philos. Mag. A* **1982**, *46*, 617.
26. Ghosal, A. K.; Biswas, S. K. *Philos. Mag. B* **1993**, *67*, 371.
27. Hamilton, G. M.; Goodman, L. E. *J. Appl. Mech.* **1966**, *33*, 371.
28. Bull, S. J.; Page, T. F. *J. Mater. Sci.* **1995**, *30*, 5356.
29. Bhattacharya, A. K.; Nix, W. D. *Int. J. Solids Struct.* **1988**, *24*, 1287.
30. Kim, N. W.; Kim, K. W.; Sin, H.-C. *Microelectron. Eng.* **2008**, *85*, 1858.
31. Chang, S.; Warren, J.; Chiang, F. P. Presented at Microscale Systems: Mechanics And Measurements Symposium, Orlando, FL, June **2000**.
32. Roy, S.; Darque-Ceretti, E.; Felder, E.; Raynal, F.; Bispo, I. *Thin Solid Films* **2010**, *518*, 3859.
33. Marques, C.; Kelly, K. W. *J. Heat Transfer* **2004**, *126*, 434.
34. Peirs, J.; Reynaerts, D.; Verplaetsen, F.; Poesen, M.; Renier, P. In Proceedings of the 16 European Conference on Solid-State Transducers, Prague, Czech, Sept **2002**; Belgium: Ku Leuven, p 790.